Focusing of acoustic waves by flat lenses made from negatively refracting two-dimensional phononic crystals

P.A. Deymier and B. Merheb
Department of Materials Science and Engineering, The University of Arizona, Tucson AZ 85721.

J.O. Vasseur
Institut d'Electronique, de Micro-électronique et de Nanotechnologie (IEMN), UMR CNRS 8520, Villeneuve d'Ascq 59652, France.

A. Sukhovich and J.H. Page
Department of Physics and Astronomy, University of Manitoba, Winnipeg, Manitoba, R3T 2N2 Canada.

Recibido el 20 de noviembre de 2007; aceptado el 5 de febrero de 2008

We investigate the phenomenon of imaging of elastic waves with flat lenses constituted of negatively refracting materials. We derive an analytical solution for the acoustic field produced by a point source near a flat lens composed of a homogeneous acoustic metamaterial (*i.e.* negative density and negative moduli) using the Green's function formalism of the Interface Response Theory. We then consider phononic crystals as a way of realizing negative refraction with materials possessing positive densities and moduli. The finite difference time domain (FDTD) simulation method is employed to investigate the properties of negative refraction and focusing of ultrasonic waves in a flat lens composed of a two-dimensional phononic crystal consisting of a triangular array of steel rods immersed in methanol. The flat lens is embedded in water. Focusing of the ultrasonic field emitted by a point source is analyzed with particular attention paid to the lateral resolution of the lens, *i.e.*, the resolution along the direction parallel to the lens' surface. The FDTD image is compared to experimental measurements of the pressure amplitude field created by a similar source and lens. Agreements and differences between the calculated and measured images as well as resolutions are reported and discussed. The flow of energy in the phononic crystal lens is calculated and matched to a simple ray tracing analysis of negative refraction in a homogeneous negatively refracting medium.

Keywords: Ultrasonic waves; phononic crystals; negative refraction.

Hemos investigado el fenómeno de imagen de ondas elásticas con lentes planos constituidos de materiales refractivos negativos. Derivamos una solución analítica para el campo acústico producido por una fuente puntual cercana a una lente plana compuesta de un metamaterial acústico homogéneo (es decir, un material con densidad y módulo negativos) usando el formalismo de la función de Green de la Teoría de Respuesta Interfacial. Después consideramos cristales fonónicos como una forma de obtener refracción negativa con materiales que poseen densidades y módulos positivos. El método de simulación de diferencias finitas en el dominio del tiempo (FDTD) es utilizado para investigar las propiedades de refracción negativa y enfocamiento de ondas ultrasónicas en una lente plana compuesta de un cristal fonónico bidimensional consistente de un arreglo triangular de barras de acero inmersas en metanol. La lente plana está inmersa en agua. El enfocamiento del campo ultrasónico emitido por una fuente puntual es analizado con atención particular a la resolución lateral de la lente, es decir, la resolución en la dirección paralela a la superficie de la lente. La imagen obtenida con el FDTD es comparada con las mediciones experimentales del campo de presiones creado por una fuente similar y una lente. Se reportan y discuten los acuerdos y las diferencias entre las imágenes calculadas y medidas así como las resoluciones. El flujo de energía en una lente de cristal fonónico es calculado y analizado como rayos de refracción negativa en un medio homogéneo refractivo negativo.

Descriptores: Ondas ultrasónicas; cristales fonónicos; refracción negativa.

PACS: 43.20.F1; 43.40.Fz

1. Introduction

Negative refraction in doubly negative electromagnetic metamaterials, introduced in the 1960's [1], continues to receive a great deal of attention. In particular, these metamaterials are compelling in view of the possibility of using negative refraction to design flat lenses that can beat the diffraction limit (so-called superlenses) [2,3]. The concept of metamaterials exhibiting negative refraction was generalized recently to acoustic waves [4]. Negative refraction in acoustic metamaterials may arise when their effective mass density and effective modulus are both negative. Such acoustic materials will exhibit a band structure that possesses bands with negative group velocity, i.e. the wave vector points in the direction opposite to the direction of propagation of the energy. With metamaterials, negative effective mass density and modulus are the result of local resonances [4,5]. Negative refraction can also be achieved using phononic crystals. Here, the mass density and the elastic moduli are positive and negative refraction results from Bragg scattering. For such phononic crystals, the elastic wave band structure exhibits a pass band with negative group velocity. Focusing of sound has been shown using lenses constituted of negatively refracting two-dimensional and three-dimensional phononic crys-

tals [6-10]. Focusing of acoustic waves by refractive acoustic devices constituted of phononic crystals was also demonstrated experimentally by Cervera et al. [11] and confirmed theoretically by Gupta and Ye [12]. Sound focusing was also achieved by flat acoustic lenses without negative refraction by using aperiodic lattices of sound scatterers [13] or by using a gradient index lens [14].

In this paper we present a comprehensive study of focusing of acoustic waves by negatively refracting flat lenses composed of a homogeneous metamaterial as well as an inhomogeneous phononic crystal. In Sec. 2, we investigate the concept of focusing using a flat lens made from a homogeneous doubly negative acoustic metamaterial by using a Green's function formalism. In that section, we derive an analytical solution for the imaged sound field of a single point source produced by the flat lens. We then consider, in Sec. 3, the focusing of acoustic waves by a flat lens made from a negatively refracting phononic crystal. This inhomogeneous system is studied by using the Finite Difference Time Domain (FDTD) method. The two-dimensional phononic crystal is a triangular lattice of steel cylinders embedded in methanol. The lens is immersed in water. Particular attention is attached to a comparison between numerical results and experimental results reported elsewhere [10]. Furthermore, we calculate the energy flux density throughout the water and lens and show that the FDTD numerical results can be related to simple ray tracing analysis of negative refraction in a homogeneous medium. Finally, Sec. 4 reports the conclusions drawn from this study.

2. Imaging with a flat lens using an acoustic metamaterial

In this section, we investigate analytically the physics of the propagation of elastic waves in a flat lens composed of a homogeneous doubly negative acoustic metamaterial. The formalism of Green's functions is used to solve for the acoustic field resulting from a point source in the vicinity of the flat lens. We first introduce the Green's function of an infinite homogeneous medium and construct the Green's function of a flat lens composed of that same medium immersed in some other medium.

The equation defining the Green's function, G, associated with elastic waves in an infinite fluid medium has the form:

$$\left(\Delta + \frac{\omega^2}{c^2}\right)\rho c^2 G(\vec{x},\vec{x}') = \delta(\vec{x}-\vec{x}') \qquad (1)$$

where Δ is the Laplace operator, δ the usual delta function, ρ and c are the density and the speed of sound in the medium, and ω the angular frequency. For a homogeneous infinite medium, the solution of equation (1) is given by:

$$G(\vec{x},\vec{x}') = \frac{-1}{4\pi\rho c^2}\frac{e^{ik|\vec{x}-\vec{x}'|}}{|\vec{x}-\vec{x}'|} \text{ where } k^2 = \frac{\omega^2}{c^2} \qquad (2)$$

For the study of lamellar composite media or media with flat surfaces or interfaces, it is convenient to write the Green's function as a two-dimensional Fourier transform:

$$G(\vec{x},\vec{x}') = \int \frac{d^2\vec{k}_{//}}{(2\pi)^2} e^{i\vec{k}_{//}(\vec{x}_{//}-\vec{x}'_{//})} G(k_{//},x_3,x'_3) \qquad (3)$$

where $\vec{k}_{//}$ and$\vec{x}_{//}$ are two-dimension vectors in the plane (x_1,x_2). Inserting equation (3) into equation (1) results in the elastic wave equation defining the two-dimensional Fourier transform of the Green's function:

$$\left(\frac{\partial^2}{\partial x_3^2} - (k^2 - k_{//}^2)\right)\rho c^2 G(k_{//},x_3,x'_3) = \delta(x_3 - x'_3) \qquad (4)$$

The solution of equation (4) is then given by:

$$G(k_{//},x_3,x'_3) = \frac{-1}{2\rho c^2\alpha} e^{-\alpha|x_3-x'_3|} \qquad (5)$$

where $\alpha^2 = k_{//}^2 - \omega^2/c^2$.

It is useful to rewrite equation (3) in the form:

$$G(\vec{x},\vec{x}') = \int\limits_{k_{//}^2 \le \frac{\omega^2}{c^2}} \frac{d^2\vec{k}_{//}}{(2\pi)^2} e^{i\vec{k}_{//}(\vec{x}_{//}-\vec{x}'_{//})} G(k_{//},x_3,x'_3) + \int\limits_{k_{//}^2 > \frac{\omega^2}{c^2}} \frac{d^2\vec{k}_{//}}{(2\pi)^2} e^{i\vec{k}_{//}(\vec{x}_{//}-\vec{x}'_{//})} G(k_{//},x_3,x'_3) \qquad (6)$$

The first term in equation (6) corresponds to an integration over $k_{//}$'s that satisfy $k_{//}^2 - \omega^2/c^2 \le 0$ and therefore includes the contribution of propagating traveling waves to the Green's function. The second integral with $k_{//}^2 - \omega^2/c^2 > 0$ is associated with evanescent waves. We note that the character of the Green's function in equation (5) in terms of traveling or evanescent waves is best seen by considering the nature of α as an imaginary or real number:

$$\alpha = \pm i\sqrt{\frac{\omega^2}{c_2} - k_{//}^2} \text{if} \omega \ge k_{//}c$$

$$\alpha = \sqrt{k_{//}^2 - \frac{\omega^2}{c_2}} \text{if } \omega \le k_{//}c \qquad (7)$$

In Eq. (7), the sign multiplying the imaginary number determines the direction of propagation of the traveling wave. Limiting the integration in Eq. (6) to traveling waves results in the so-called diffraction limit.

We now consider the calculation of the Green's function of inhomogeneous media. The Interface Response Theory (IRT) [15] allows for the construction of the Green's function of an inhomogeneous medium in terms of the Green's functions of the block constituents of the composite. The Green's function of a composite medium can be written in the form

of an interface integral equation:

$$\begin{aligned}&\overleftrightarrow{g}(\mathbf{r},\mathbf{r}') = \overleftrightarrow{G}(\mathbf{r},\mathbf{r}') + \int d\mathbf{r}_M \overleftrightarrow{G}(\mathbf{r},\mathbf{r}_M) \int d\mathbf{r}'^{-1}_M \overleftrightarrow{G}(\mathbf{r}_M,\mathbf{r}'_M)\\ &\times \int d\mathbf{r}''_M \left[\overleftrightarrow{g}(\mathbf{r}'_M,\mathbf{r}''_M) - \overleftrightarrow{G}(\mathbf{r}'_M,\mathbf{r}''_M)\right]\\ &\times \int d\mathbf{r}'''_M \overleftrightarrow{G}^{-1}(\mathbf{r}''_M,\mathbf{r}'''_M)\overleftrightarrow{G}(\mathbf{r}'''_M,\mathbf{r}'),\\ &\{\mathbf{r},\mathbf{r}'\} \in D,\\ &\{\mathbf{r}_M,\mathbf{r}'_M,\mathbf{r}''_M,\mathbf{r}'''_M\} \in M\end{aligned} \tag{8}$$

with

$$\overleftrightarrow{G}(\mathbf{r},\mathbf{r}') = \begin{cases} \overleftrightarrow{G}_i(\mathbf{r},\mathbf{r}'),\ \{\mathbf{r},\mathbf{r}'\} \in D_i,\ i = 1,N \\ 0\ \mathbf{r} \in D_i,\ \mathbf{r}' \in D_j,\ i \neq j \end{cases} \tag{9}$$

where D represents the space of the entire inhomogeneous medium, M is the total domain of interfaces and D_i is the space in which the constitutive block i is defined. In the case of layered composites media, using the two-dimensional Fourier transforms of the Green's function in a plane parallel to the interfaces, the domain of the interfaces reduces to points along the x_3 axis; thus, the integrals in equation (8) reduce to discrete sums over these points.

We note that in order to solve for $\overleftrightarrow{g}(\mathbf{r},\mathbf{r}')$ using Eq. (8), one needs to know its form in the domain of the interfaces, $\overleftrightarrow{g}(\mathbf{r}_M,\mathbf{r}''_M)$. According to the IRT, the inverse of the Green's function of the inhomogeneous medium defined in the domain of the interfaces may be expressed in terms of the inverse Green's function of the constitutive blocks defined in the domain of their surfaces, such that

$$\begin{aligned}&\overleftrightarrow{g}^{-1}(\mathbf{r} \in M_{ij},\mathbf{r}' \in M_{kl}) = 0\\ &\text{if } M_{kl} \notin M_i\\ &\overleftrightarrow{g}^{-1}(\mathbf{r} \in M_{ij},\mathbf{r}' \in M_{il}) = \overleftrightarrow{g}_s^{-1}(\mathbf{r} \in M_{ij},\mathbf{r}' \in M_{il})\\ &\text{if } l \neq j\\ &\overleftrightarrow{g}^{-1}(\mathbf{r} \in M_{ij},\mathbf{r}' \in M_{ij}) = \sum_k \overleftrightarrow{g}_s^{-1}(\mathbf{r} \in M_{kl},\mathbf{r}' \in M_{kl})\\ &\text{if } M_{kl} \equiv M_{ij}\end{aligned} \tag{10}$$

with M_{ij}standing for the interface between the constitutive blocks i and j. In equation (10), $\overleftrightarrow{g}_s$ stands for the Green's function of the constitutive blocks with free surfaces.

All the boundary conditions (*e.g.* continuity of displacement) at the interfaces are satisfied through equations (10). The inhomogeneous media considered in this study are composed of semi-infinite media and slabs. The Green's function of a semi-infinite medium or a slab is obtained from the bulk Green's function defined previously. In the presence of a free surface or free surfaces, Eq. (4) has to be solved subject to the boundary conditions expressing the absence of stress at the surface. The inverse of the Green's function at the surface of a semi-infinite fluid elastic medium and at the surfaces of an elastic fluid slab have been reported in the literature and presented below.

The inverse of the Green's function, $\overleftrightarrow{g}_s^{-1}$ of a semi-infinite medium i, bounded by a free surface at $x_3 = 0$, is given in the domain of its surface by [16]:

$$g_{si}^{-1}(k_{//}\omega\,|x_3 = 0, x'_3 = 0\,) = -\rho_i\alpha_i c_i^2 \tag{11}$$

In the construction of a flat lens, we will also consider a slab of some medium 1 of thickness, d, with surfaces perpendicular to the axis x_3 and located at $x_3 = \pm d/2$. The inverse Green's function of the slab in the space of its surfaces has been derived previously [17] and is given by

$$\begin{aligned}&\overleftrightarrow{g}_{s1}^{-1}(MM)\\ &= \begin{pmatrix} \overleftrightarrow{g}_{s1}^{-1}\left(k_{//}\omega\,|-\frac{d}{2},-\frac{d}{2}\right) & \overleftrightarrow{g}_{s1}^{-1}\left(k_{//}\omega\,|-\frac{d}{2},+\frac{d}{2}\right) \\ \overleftrightarrow{g}_{s1}^{-1}\left(k_{//}\omega\,|+\frac{d}{2},-\frac{d}{2}\right) & \overleftrightarrow{g}_{s1}^{-1}\left(k_{//}\omega\,|+\frac{d}{2},+\frac{d}{2}\right) \end{pmatrix}\\ &= \begin{pmatrix} \nu & w \\ w & \nu \end{pmatrix}\end{aligned} \tag{12}$$

Its components take the analytical form

$$\begin{aligned} v &= -\rho_1\alpha_1 c_1^2 \frac{ch\,(\alpha_1 d)}{sh\,(\alpha_1 d)}\\ w &= -\rho_1\alpha_1 c_1^2 \frac{(-1)}{sh\,(\alpha_1 d)}\end{aligned} \tag{13}$$

We now consider the inhomogeneous medium consisting of a medium 1 sandwiched between two semi-infinite media 2 (see Fig. 1). The interfaces between these media are parallel to each other and normal to the axis x_3. This geometry is that of a flat lens (1) immersed in some medium 2. The thickness of the lens is defined as d. The lens is centered on the origin 0.

Using the IRT to calculate the Green's function of the composite medium in terms of the Green's functions of the constitutive parts, namely a slab of medium 1 and the two semi-infinite media, we obtain:

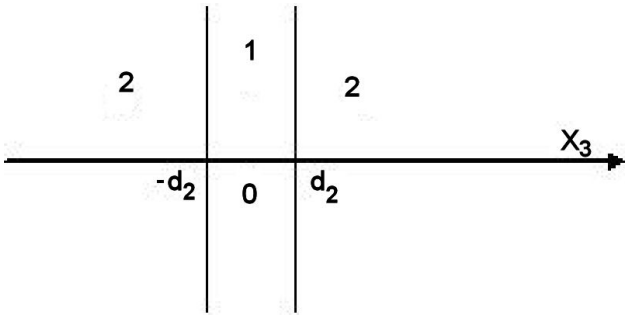

FIGURE 1. Schematic geometrical representation of the composite medium representative of a flat lens (medium 1) immersed in some medium 2.

$$g(k_{//},x_3,x'_3) = \frac{2\rho_1 c_1^2\alpha_1 e^{-\alpha_2(x_3-x'_3-d)}}{\left(\rho_1 c_1^2\alpha_1 + \rho_2 c_2^2\alpha_2\right)^2 e^{\alpha_1 d} - \left(\rho_1 c_1^2\alpha_1 - \rho_2 c_2^2\alpha_2\right)^2 e^{-\alpha_1 d}} \text{ for } x'_3 < -d/2 \text{ and } x_3 > d/2 \tag{14}$$

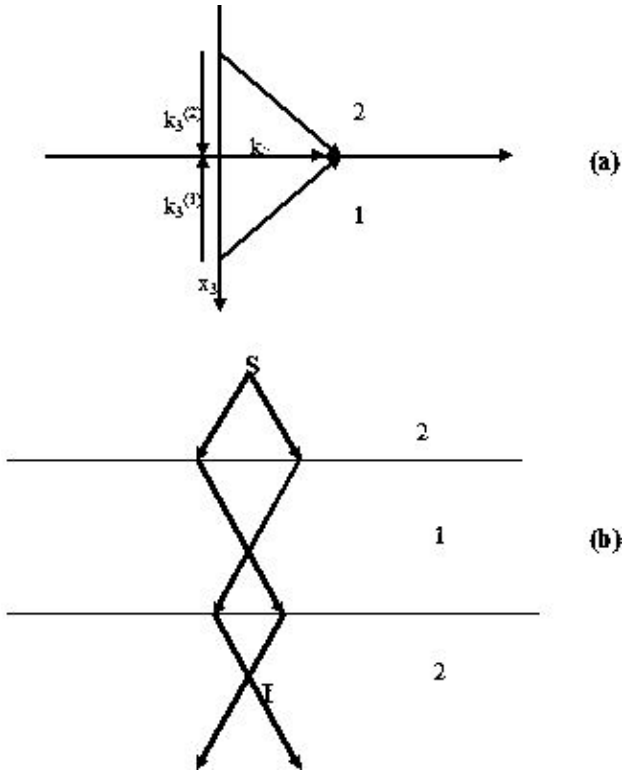

FIGURE 2. (a) Schematic illustration of negative refraction across an interface between a regular medium (2) and a doubly negative (density, modulus) metamaterial. $k_{//}$, α_1 and α_2 are the components of the wave vector parallel and perpendicular to the interface between the media 2 and 1, respectively. (b) Schematic illustration of focusing by a flat lens exhibiting negative refraction [medium (1)]. S and I are the source and image, respectively.

In Eq. (14), the subscripts 1 and 2 refer to the two media. Medium 2 is considered to be a normal positively refracting fluid with

$$\alpha_2 = \sqrt{k_{//}^2 - \frac{\omega^2}{c_2^2}} \text{ if } \omega \leq k_{//}c_2$$

$$\alpha_2 = -i\sqrt{\frac{\omega^2}{c_2^2} - k_{//}^2} = -ik_3^{(2)} \text{ if } \omega \geq k_{//}c_2 \qquad (15)$$

In Eq. (15), the negative sign multiplying the imaginary number ensures a propagating character to the elastic waves in medium 2.

When medium 1 is composed of an acoustic metamaterial exhibiting negative refraction, $\rho_1 \leq 0$. Since the speed of sound in the medium 1, $c_1 = \sqrt{\lambda/\rho}$, is positive and real, the compressibility must be negative, $\lambda < 0$. For this metamaterial, we have:

$$\alpha_1 = \sqrt{k_{//}^2 - \frac{\omega^2}{c_1^2}} \text{ if } \omega \leq k_{//}c_1$$

$$\alpha_1 = +i\sqrt{\frac{\omega^2}{c_1^2} - k_{//}^2} = +ik_3^{(1)} \text{ if } \omega \geq k_{//}c_1 \qquad (16)$$

The positive sign multiplying the imaginary number "i" indicates that a wave, which propagates from medium 2 into medium 1 and which satisfies the continuity of $k_{//}$ at the interface between the two media, would have components of the wave vector along the x_3 direction antiparallel to each other. Since the energy of the wave propagates along the same direction (*i.e.* the direction of the group velocity), this implies that the wave vector in medium 2 is parallel to the group velocity and that in medium 1 the wave vector is antiparallel to the group velocity. This behavior is characteristic of the phenomenon of negative refraction at the interface between media 1 and 2 and is illustrated in Fig. 2.

For the sake of simplicity and in order to obtain analytical solutions, we take $\rho_1 = -\rho_2 = -\rho \leq 0, c_1 = c_2 = c$. We also consider the separate cases of traveling and evanescent waves. For traveling waves, $k_{//} \leq \omega/c$ and $\alpha_1 = -\alpha_2 = -\alpha$. Under these conditions, the Green's function of the composite medium simplifies to

$$g(k_{//}, x_3, x_3') = \frac{e^{-\alpha(x_3 - x_3' - 2d)}}{2\rho c^2 \alpha}$$
$$\text{for } x_3' < -d/2 \text{ and } x_3 > d/2 \qquad (17)$$

We are now going to analyze the response of the composite medium to a δ stimulus (*i.e.* point source) applied on the left side of the slab of medium 1 located at $x_3' = -a - d/2$. We are particularly interested in the nature of the Green's function on the right side (side opposite to the point source) of the slab. In that case the position-dependent term in the argument of the exponential in Eq. (17) becomes $x_3 - x_3' - 2d = x_3 - (3(d/2) - a)$. Considering the response at $x_3 \geq 3(d/2) - a$ then $x_3 - (3(d/2) - a) = |x_3 - (3(d/2) - a)|$. With this, Eq. (17) is rearranged in the form:

$$g(k_{//}, x_3, x_3') = \frac{e^{-\alpha\left|x_3 - \left(\frac{3d}{2} - a\right)\right|}}{2\rho c^2 \alpha}$$
$$\text{for } x_3' = -a - d/2 \text{ and } x_3 > 3\frac{d}{2} - a \qquad (18)$$

In the case of evanescent waves, $k_{//} > \omega/c$ and $\alpha_1 = \alpha_2 = \alpha$, Eq. (14) takes again the form of Eq. (17). Therefore, for all $k_{//}$, the Green's function at $x_3' = -a - d/2$ and $x_3 > 3(d/2) - a$ (*i.e.* Eq. (18)), is isomorphic to the two-dimensional Fourier transform of the Green's function of a homogeneous medium (see Eq. (5)). Taking the inverse Fourier transformation over all $k_{//}$ (*i.e.* traveling and evanescent waves) gives a solution of the form: $G(\vec{x}, \vec{x}_i) = (1/4\pi\rho c^2)(e^{i(\omega/c)|\vec{x} - \vec{x}_i|})|\vec{x} - \vec{x}_i|$ where $\vec{x}_i = (0, 0, (3d/2) - a)$ is the focal point of a perfect image of the source. Limiting the integration in Eq. (6) to traveling waves only (evanescent waves have exponentially decaying amplitudes) results in an imperfect image with a resolution (half width of image) exceeding the ultimate resolution of half the wavelength as predicted by diffraction theory.

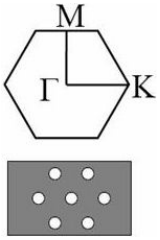

FIGURE 3. Schematic illustration of the phononic crystal composed of a triangular array of steel cylindrical inclusions in a methanol matrix. The first Brillouin zone of that crystal is also illustrated.

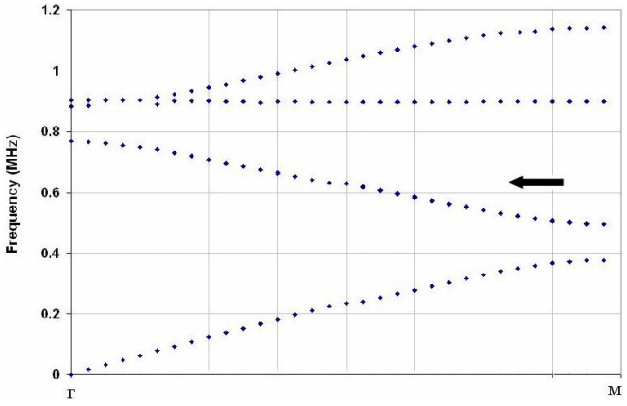

FIGURE 4. Band structure of the phononic crystal in the direction ΓM of the Brillouin zone. The band marked with an arrow shows a negative group velocity.

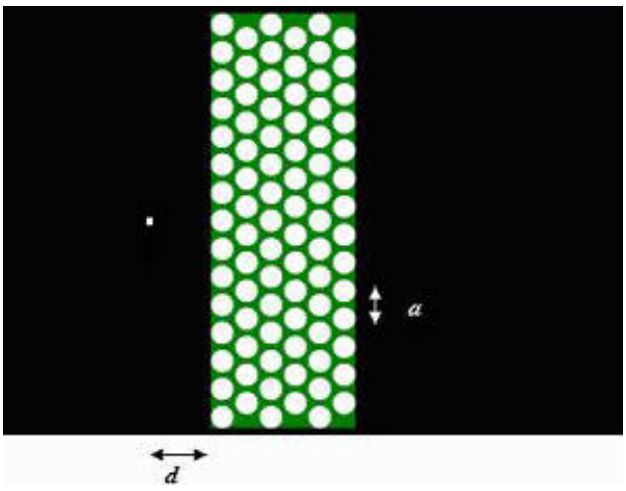

FIGURE 5. Schematic illustration of the phononic crystal flat lens. The lens is made from six planes of cylinders perpendicular to the ΓM direction. The lens is finite in the direction perpendicular to the ΓM direction with a length of approximately $15a$ where a is the inter-cylinder spacing. The white spot marks the location of the source of sound at some distance d from the left side of the lens surface.

3. Acoustic imaging using a flat lens made out of a phononic crystal

We have shown in Sec. 2 that a flat lens composed of a homogeneous acoustic metamaterial can focus sound waves with a resolution that approaches the limit imposed by diffraction. Here we use numerical methods to investigate the focusing of sound by an inhomogeneous flat lens composed of a phononic crystal. Phononic crystals composed of materials with positive densities and moduli can exhibit negative refraction. In contrast to homogeneous metamaterials, negative refraction in the case of phononic crystals results from band structure effects associated with Bragg scattering due to the periodic nature of the lattice. We employ the Finite Difference Time Domain method to study the negative refraction and focusing properties of a two-dimensional phononic crystal. The FDTD method has been extensively used to study the propagation of acoustic waves in phononic crystals [18-20]. The wave equation to be solved in two-dimensions (x_1,x_3) is:

$$\rho(x_1, x_3)\frac{\partial^2 \vec{u}}{\partial t^2} = \nabla.\sigma \tag{19}$$

where $\rho(x_1, x_3)$ is the mass density, $\vec{u}$ and σ are the two-dimensional displacement field and the stress tensor. The components of the stress tensor are calculated from the elastic displacement using isotropic Hooke's laws with position dependent elastic coefficients $C_{11}(x_1,x_3)$ and $C_{44}(x_1,x_3)$. The latter elastic coefficient is zero for fluids. The FDTD method can also be extended to calculate the band structure of inhomogeneous periodic medium [21]. In all the calculations reported below, we use an interval for the discretization of space of 2×10^{-5}m. The acoustic waves are propagated in time with a time step of 6×10^{-10}sec. These values satisfy the Courant condition and lead to a stable algorithm.

We consider a two-dimensional phononic crystal composed of a triangular array of steel cylinders embedded in a matrix of methanol (Fig. 3). The inter-cylinder spacing is taken as 1.27mm with a cylinder diameter of 1.02mm. The steel physical characteristics are: mass density of 7780kg/m^3, longitudinal speed of sound of 5825m/s and transverse speed of sound of 3227m/s. For the methanol matrix, we use a mass density of 792kg/m^3 and a longitudinal speed of sound of 1103m/s. Finally, all calculations of the lens immersed in water employ for that fluid a mass density equal to 1000kg/m^3 and a speed of sound of 1500m/s. The band structure of the periodic phononic crystal is reported in figure 4. It exhibits a pass band between 500kHz and 778kHz with a negative group velocity. This band corresponds to waves with a wave vector pointing in the direction opposite to the direction of propagation of the energy. It has been shown experimentally that waves in this band exhibit the phenomenon of negative refraction upon crossing an interface between a homogeneous medium such as water and the phononic crystal [10]. The equifrequency contour in the Brillouin zone of the phononic crystal matches that of water at a frequency of

550 kHz [10]. The latter condition is important to achieve good imaging with the phononic crystal flat lens, as all incident waves will be refracted and will contribute to the construction of an image. In the following, the imaging capability of the steel/methanol flat lens will be studied in water. We now develop the model of a lens that we will compare with experimental results reported in reference 10. The experiment involves the mapping of the pressure field amplitude created by a 550 kHz line source transducer (0.55mm wide) and imaged by a steel/methanol phononic crystal flat lens. The line source runs parallel to the principal axis of the steel cylinders and mimics the behavior of a point source in a plane perpendicular to the cylinders. To model this system we utilize the method of FDTD to study the propagation of acoustic waves emitted from a point source, having the size of a grid point in the FDTD discretized mesh, located at a distance d=1.6mm from the lens surface (Fig. 5). The source emits a sinusoidal displacement which is updated in time according to:

$$u_1^u = u_1 + A\sin(\omega t)$$
$$u_3^u = u_3 + A\cos(\omega t) \qquad (20)$$

where $\vec{u}^u$ is the updated displacement field of the point source and $\vec{u}$ is the solution to equation 19; A is the amplitude of the sinusoidal source and ω its angular frequency.

Because of a discrepancy between the FDTD band structure of the model and the experimental one, possibly due to the choice of the physical parameters or discretization mesh used in the model, the condition for matching the equifrequency contour of the Brillouin zone of the model phononic crystal to that of water is achieved at a frequency of 530kHz and not 550kHz as in the experiment. The point source used in the FDTD calculation is therefore emitting a sound wave at a frequency of 530kHz. We impose Mur's absorbing boundary conditions [22] along the four edges of the simulated system. In Fig. 6, we report the calculated average pressure field on the side of the lens opposite to the source in the form of a contour map. The average pressure is normalized to the maximum average pressure on that side of the lens. The average pressure is defined at steady state according to the relation:

$$\bar{P} = \frac{\pi}{2}\frac{1}{T}\int_t^{t+T} |P(t)|\, dt \qquad (21)$$

where the time integral is taken over one period of the incident wave, T, and the instantaneous pressure, $P(t)$, is calculated from the stress tensor according to

$$P(t) = -\frac{1}{2}(\sigma_{11} + \sigma_{22}).$$

Figure 6 clearly shows that the negatively refracting phononic crystal behaves as a lens and focuses the sound emitted by the source into a localized image. The calculated image is compared to the experimental results of [10] in Fig. 7 in the form of lateral and perpendicular cuts of the contour map through

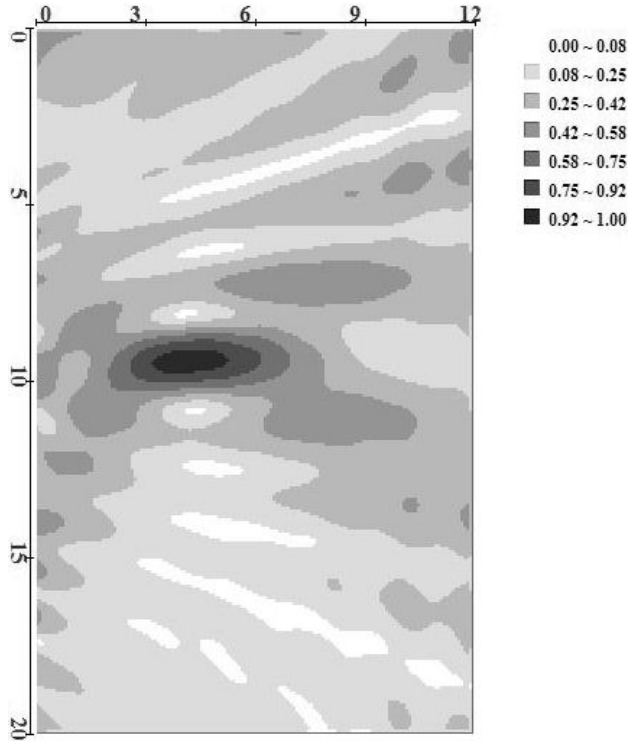

FIGURE 6. Contour map of the normalized average pressure field (see text for definition) on the side of the lens opposite to the source of sound. The units of the axes are in millimeters.

the point of highest normalized average pressure. Good agreement is observed for the width of the focal spot in the direction parallel to the crystal surface while along the perpendicular direction, we find experimentally that the focal spot is narrower and closer to the crystal surface than in the theoretical predictions. According to the Rayleigh criterion, the spatial resolution of the lens can be estimated as half the width of the peak, measured from the maximum to the first zero. In the experimental case, this width amounts to 1.5mm. The wavelength of the experimental incident wave at 550kHz in water is λ=2.73mm. The experimental spatial resolution of the flat lens is therefore 0.55λ. With a half peak width of 2.77mm and the frequency of 530kHz, the resolution of the model lens is 0.49λ. This resolution is just below than the ultimate resolution limit of 0.5λ of any conventional imaging system as predicted by diffraction theory.

To shed further light on the path of propagation of acoustic waves in the methanol/steel phononic crystal lens, we have calculated the energy flux density vector throughout the simulated water-methanol/steel lens system. The energy flux density is defined as $\vec{R} = P\vec{v}$ where P is the pressure and $\vec{v}$ is the group velocity. The energy flux density vector points in the direction of the group velocity. We report in figure 8 contour maps of the components of $\vec{R} = (R_1, R_3)$ averaged over one period. Figure 8b shows that the R_3 component is essentially positive in the lens as well as the water region to the right of the lens, that is the energy propagates in the positive direction along the axis x_3 (*i.e.* from the left to the right).

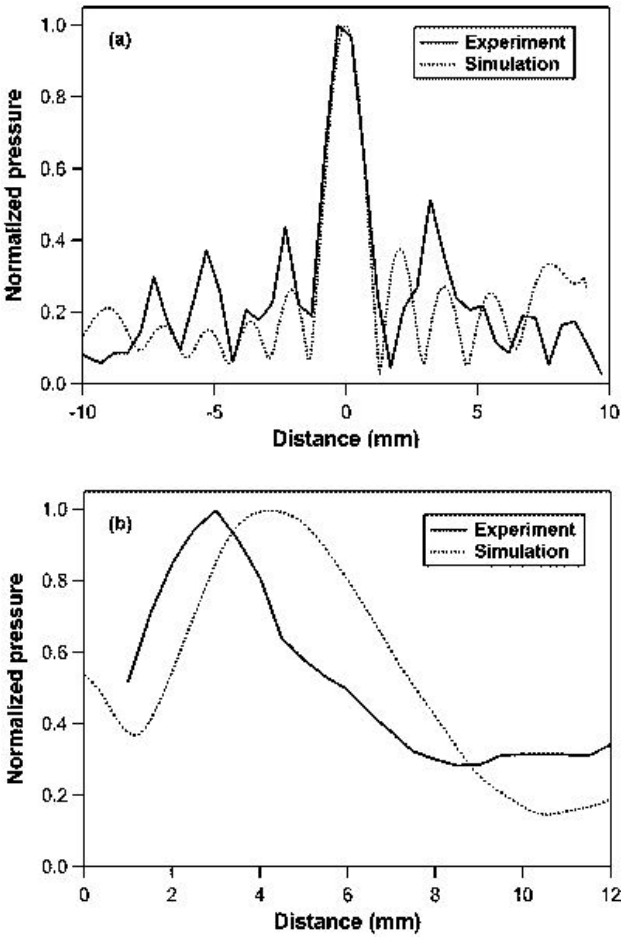

FIGURE 7. Experimental (solid line) and calculated (dotted line) normalized average pressure on the image side of the lens through the point of highest normalized pressure (1) along (a) the direction parallel and (b) the direction perpendicular to the lens surface, respectively. The horizontal axes are in units of millimeters. The main peak width in (a) is 3.0mm for the experimental data and 2.77mm for the calculated one. The measured half width corresponds to a resolution of the lens of 0.55λ where λ is the wavelength of the incident wave in water. The resolution of the model lens of 0.49λ is just below the ultimate resolution limit of 0.5λ of any conventional imaging system as predicted by diffraction theory. In (a), the position of the peaks is centered on $x = 0$ to facilitate comparison of the experimental and calculated peak shapes.

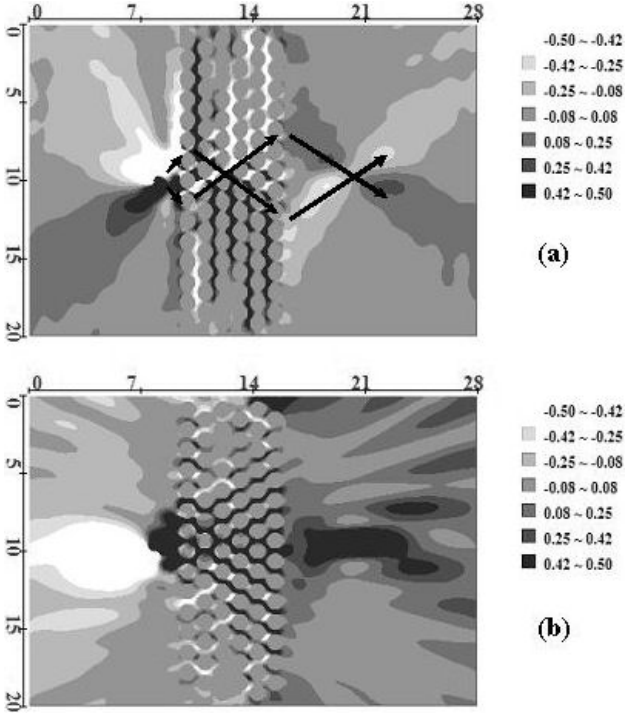

FIGURE 8. Contour maps of the energy flux density vector, (a) component, R_1, parallel to the surface of the lens, and (b) component, R_3, perpendicular to the surface of the lens. The axes are in units of millimeters. Note that the positive direction of the x_1 axis parallel to the lens points down. The arrows in (a) are guides to the eye illustrating the direction of the propagation of energy.

More interestingly, the component R_1 changes sign successively as one moves from the source to the lens, through the lens and out into water. We have superposed arrows onto Fig. 8a to illustrate the overall direction of propagation of the energy. Acoustic waves diverging from the source are refracted negatively at the left surface of the lens. Inside the lens from left to right, the waves converge back into a "point" and diverge beyond. Upon exit through the second surface the diverging waves are refracted negatively a second time and focused into an image to the right of the lens. This is the path a wave would follow in a ray tracing representation of focusing by a negatively refracting homogeneous flat lens as described in Sec. 2 and Fig. 2b. Furthermore, it is worth noting that the energy propagates mostly in the methanol matrix of the phononic crystal lens and that the steel cylinders behave essentially like rigid rods.

For phononic crystal lenses periodic in the direction parallel to the lens surface with a period a_s, the image obtained is constructed from waves with a wave vector $k_{//}$ limited by $k_s=\pi/a_s$ [3]. Here, a_s=1.27mm and k_s=2.47mm^{-1}. Considering equation (6), the wave vector limit for traveling waves is $k_{//}=\omega/c$ which for water at 530kHz amounts to approximately 2.22mm^{-1}¡k_s, implying that the image that we observe in the FDTD calculation includes all traveling waves. That is, the resolution of the lens is not limited by its surface periodicity.

4. Conclusions

We have investigated the phenomenon of negative refraction and focusing of acoustic waves by a flat lens composed of a homogeneous metamaterial exhibiting negative effective mass and compressibility using the Green's function formalism of the Interface Response Theory. The Finite Difference Time Domain (FDTD) method is also used to show that a flat lens constituted of a phononic crystal can be used to focus sound waves. The requisite for focusing is the existence of a band in the band structure of the phononic crystal that exhibits a negative group velocity. We compare the FDTD

image with experimental data reported elsewhere [10]. Satisfactory agreement between the numerical results and experimental results is found in the width of the image produced by the phononic crystal lens. Through the calculation of the energy flux density we relate the path of energy in the phononic crystal lens to the simple ray tracing representation of negative refraction and focusing in a homogeneous metamaterial lens. We also show that the resolution of the lens approaches the limit of diffraction and is not limited by the phononic crystal surface periodicity.

1. V.G. Veselago, *Sov. Phys. Usp.* **10** (1968) 509.
2. J.B. Pendry, *Phys. Rev. Lett.* **85** (2000) 3966.
3. C. Luo, S.G. Johnson, and J.D. Joannopoulos, *Phys. Rev. B* **68** (2003) 045115.
4. J. Li, K.H. Fung, Z.Y. Liu, P. Sheng, and C.T. Chan, in *Physics of Negative Refraction and Negative Index Materials*, Springer Series in Materials Science (Springer Berlin Heidelberg 2007) Chapter 8, Vol. 98.
5. P. Sheng, J. Mei, Z. Liu, and W. Wen, *Physica B* **394** (2007) 256.
6. S. Yang *et al.*, *Phys. Rev. Lett.* **93** (2004) 024301.
7. J.H. Page *et al.*, *Phys. Stat. Sol. (b)* **241** (2004) 3454.
8. K. Imamura and S. Tamura, *Phys. Rev. B* **70** (2004) 174308.
9. M. Ke *et al.*, *Solid State Comm.* **142** (2007) 177.
10. A. Sukhovich, L. Jing, and J. Page, *Phys. Rev. B* **77** (2008) 014301.
11. F. Cervera *et al.*, *Phys. Rev. Lett.* **88** (2002) 023902.
12. B.C. Gupta and Z. Ye, *Phys. Rev. E* **67** (2003) 036603.
13. A. Hakansson, F. Cervera, and J. Sánchez-Dehesa, *Appl. Phys. Lett.* **86** (2005) 054102.
14. D. Torrent and J. Sánchez-Dehesa, *New J. Phys.* **9** (2007) 323.
15. L. Dobrzynski, *Surf. Sci.* **180** (1987) 489.
16. L. Dobrzynski, *Surf. Sci. Reports* **11** (1990) 139.
17. L. Dobrzynski, J. Mendialdua, A. Rodriguez, S. Bolibo and M. More, *J. Phys. France* **50** (1989) 2563.
18. D. Garcia-Pablos *et al.*, *Phys. Rev. Lett.* **84** (2000) 4349.
19. J.O. Vasseur *et al.*, *Phys. Rev. Lett.* **86** (2001) 3012.
20. T. Miyashita and C. Inoue, *Jpn. J. Appl. Phys. Part1* **40** (2001) 3488.
21. Y. Tanaka, Y. Tomoyasu, and S. Tamura, *Phys. Rev. B* **62** (2000) 7387.
22. G. Mur, *IEEE Trans. Electromagn. Comput.* **23** (1981) 377.